Eur. Phys. J. C (2009) 60: 181–196
DOI 10.1140/epjc/s10052-009-0930-5

THE EUROPEAN PHYSICAL JOURNAL C

Regular Article - Experimental Physics

Study of moments of event shapes and a determination of α_S using e^+e^- annihilation data from JADE

C. Pahl[1,2,a], **S. Bethke**[1], **S. Kluth**[1], **J. Schieck**[1], **The JADE Collaboration**[b]

[1]Max-Planck-Institut für Physik, Föhringer Ring 6, 80805, Munich, Germany
[2]Excellence Cluster Universe, Technische Universität München, Boltzmannstr. 2, 85748, Garching, Germany

In memory of Beate Naroska

Received: 15 October 2008 / Revised: 14 January 2009 / Published online: 21 February 2009

Abstract Data from e^+e^- annihilation into hadrons, collected by the JADE experiment at centre-of-mass energies between 14 GeV and 44 GeV, are used to study moments of event shape distributions. Models with hadronisation parameters tuned to the LEP 1 precision data provide an adequate description of the low energy data studied here. The NLO QCD calculations, however, show systematic deficiencies for some of the moments. The strong coupling measured from the moments which are reasonably described by NLO QCD,

$$\alpha_S(M_{Z^0}) = 0.1287 \pm 0.0007(\text{stat.}) \pm 0.0011(\text{exp.}) \pm 0.0022(\text{had.}) \pm 0.0075(\text{theo.}),$$

is consistent with the world average.

PACS 12.38.Bx · 12.38.Qk

1 Introduction

Electron-positron annihilation into hadrons constitutes a precise testing ground of Quantum Chromodynamics (QCD). Commonly jet production rates or distributions of event shape variables have been studied. Predictions of perturbative QCD combined with hadronisation corrections derived from models have been found to describe the data at low and high energies well, see e.g. [2–6].

In this analysis we use data from the JADE experiment, recorded in the years 1979 to 1986 at the PETRA e^+e^- collider at DESY at six centre-of-mass (c.m.) energies $\sqrt{s}$ covering the range 14–44 GeV. We measure the first five moments of event shape variables for the first time in this low $\sqrt{s}$ region of e^+e^- annihilation and compare the data to predictions by Monte Carlo (MC) models and by perturbative QCD. Moments sample all phase space, but are more sensitive to specific parts of phase space, dependent on their order. From the comparison of the data with theory we extract the strong coupling α_S. The measurement of the moments, as well as the α_S determination, follow closely the analysis by the OPAL experiment in the complete LEP energy range of 91–209 GeV [7]. This work supplements our previous analyses on jet production rates, determinations of α_S and four jet production, using JADE and OPAL data [3, 8, 9].

The outline of the paper is as follows. In Sect. 2, we present the observables used in the analysis and describe the perturbative QCD predictions. In Sect. 3 the analysis procedure is explained in detail. Section 4 contains the discussion of the systematic checks which are performed and the resulting systematic errors. We collect the results and describe the determination of α_S in Sect. 5, and we summarize in Sect. 6.

2 Observables

Event shape variables are a convenient way to characterise properties of hadronic events by the distribution of particle momenta. For the definition of the variables we refer to [7]. The event shapes considered here are Thrust T, C-parameter C, Heavy Jet Mass M_H, jet broadening variables B_T and B_W, and the transition value between 2 and 3 jets in the Durham jet scheme, y_{23}^D. The α_S determination in [7] is based on distributions and moments of these variables. Their theoretical description is currently the most advanced [10–12]. Further, we measure moments of Thrust major T_{maj}, Thrust minor T_{min}, Oblateness O, Sphericity S, Light Jet Mass M_L, and Narrow Jet Broadening B_N. Moments of these variables and

[a] e-mail: pahl@mppmu.mpg.de

[b] See [1] for the full list of authors.

variances of all measured event shapes will be made available in the HEPDATA database.[1]

Generic event shape variables y are constructed such that spherical and multi-jet events yield large values of y, while two narrow back-to-back jets yield $y \simeq 0$. Thrust T is an exception to this rule. By using $y = 1 - T$ instead the condition is fulfilled for all event shapes.

The nth, $n = 1, 2, \ldots$, moment of the distribution of the event shape variable y is defined by

$$\langle y^n \rangle = \int_0^{y_{\max}} y^n \frac{1}{\sigma} \frac{\mathrm{d}\sigma}{\mathrm{d}y} \mathrm{d}y, \tag{2.1}$$

where $y_{\max}$ is the kinematically allowed upper limit of the variable y.

Predictions have been calculated for the moments of event shapes. Their evolution with c.m. energy allows direct tests of the predicted energy evolution of the strong coupling α_S. Furthermore we determine $\alpha_S(M_{Z^0})$ by evolving our measurements to the energy scale given by the mass of the Z^0 boson. The theoretical calculations involve a integration over full phase space, which implies that comparison with data always probes all of the available phase space. This is in contrast to QCD predictions for distributions; these are commonly only compared with data—e.g. in order to measure α_S—in restricted regions, where the theory is well defined and describes the data well, see e.g. [2]. Comparisons of QCD predictions for moments of event shape distributions with data are thus complementary to tests of the theory using distributions.

Uncertainties in the NNLO predictions for event shape distributions in the two-jet region [11, 12] prevent the reliable calculation of moments to NNLO at present, and therefore we compare with NLO predictions only. The QCD prediction of $\langle y^n \rangle$ at parton level, in next-to-leading order (NLO) perturbation theory, and with $\bar{\alpha}_S \equiv \alpha_S/(2\pi)$, is

$$\langle y^n \rangle^{\mathrm{part,theo}} = \mathcal{A}_n \bar{\alpha}_S + (\mathcal{B}_n - 2\mathcal{A}_n)\bar{\alpha}_S^2. \tag{2.2}$$

The values of the coefficients[2] $\mathcal{A}_n$ and $\mathcal{B}_n$ can be obtained by numerical integration of the QCD matrix elements using the program EVENT2 [13].

The coupling $\bar{\alpha}_S$ and the $\bar{\alpha}_S^2$ coefficient depend on the renormalisation scale μ [14]. For the sake of clarity the renormalisation scale factor is defined as $x_\mu \equiv \mu/\sqrt{s}$, so setting x_μ to one implies that the renormalisation scale is $\sqrt{s}$. A truncated fixed order QCD calculation such as equation (2.2) will then depend on x_μ. The renormalisation scale dependence is implemented by the replacement $\mathcal{B}_n \to \mathcal{B}_n + \beta_0 \ln(x_\mu)\mathcal{A}_n$ where $\beta_0 = 11 - \frac{2}{3}n_f$ is the leading order β-function coefficient of the renormalisation group equation and $n_f = 5$ is the number of active quark flavours.

3 Analysis procedure

3.1 The JADE detector

The JADE detector is described in detail in [1]. Energy measurement by the electromagnetic calorimeter and the reconstruction of charged particle tracks in the central track detector are the main ingredients for this analysis. The central jet chamber was positioned in an axial magnetic field of 0.48 T provided by a solenoidal magnet.[3] The magnet coil was surrounded by the lead glass calorimeter, which measured electromagnetic energy and consisted of a barrel and two endcap sections.

3.2 Data samples

In this analysis we are using data samples identical to the samples used in [1–4, 8, 15], collected by the JADE experiment between 1979 and 1986; they correspond to a total integrated luminosity of ca. 195 pb^{-1}. Table 3.1 contains the breakdown of the data samples—data taking period, energy range, mean centre-of-mass energy, integrated luminosity and the number of selected hadronic events.

3.3 Monte Carlo samples

To correct the data for experimental effects and backgrounds we use samples of MC simulated events. Using PYTHIA 5.7 [16] we simulate the process $\mathrm{e^+e^-} \to$ hadrons. For systematic checks we use corresponding samples obtained by simulation with HERWIG 5.9 [17]. We process

Table 3.1 Year of data taking, energy range, integrated luminosity, average centre-of-mass energy and the numbers of selected data events for each data sample

Year	Range of $\sqrt{s}$ in GeV	$\sqrt{s}$ mean in GeV	Luminosity (pb^{-1})	Selected events
1981	13.0–15.0	14.0	1.46	1783
1981	21.0–23.0	22.0	2.41	1403
1981–1982	33.8–36.0	34.6	61.7	14313
1986	34.0–36.0	35.0	92.3	20876
1985	37.3–39.3	38.3	8.28	1585
1984–1985	43.4–46.4	43.8	28.8	4376

[1] http://durpdg.dur.ac.uk/HEPDATA/.

[2] The $\bar{\alpha}_S^2$ coefficient is written as $\mathcal{B}_n - 2\mathcal{A}_n$ because the QCD calculations are normalized to the Born cross section σ_0, while the data are normalized to the total hadronic cross section, $\sigma_{\mathrm{tot}} = \sigma_0(1 + 2\bar{\alpha}_S)$ in LO.

[3] In the JADE right-handed coordinate system the $+x$ axis pointed towards the centre of the PETRA ring, the y axis pointed upwards and the z axis pointed in the direction of the positron beam. The polar angle θ and the azimuthal angle ϕ were defined with respect to z and x, respectively, while r was the distance from the z-axis.

the MC samples generated at each energy point through a full simulation of the JADE detector [18–20], summarized in [15]; and we reconstruct them in essentially the same way as the data.

Using the parton shower models PYTHIA 6.158, HERWIG 6.2 [21] and ARIADNE 4.11 [22] we employ in addition large samples of MC events without detector simulation, in order to compare with the corrected data. For the purpose of comparison with the data, the MC events include the effects of hadronisation, i.e. the transition of partons into hadrons. All used major versions of the models were adjusted to LEP 1 data by the OPAL collaboration [23, 24], so we expect comparable results from them.

3.4 Selection of events

The selection—identical to the one used in [8]—aims at selecting hadronic events in the JADE data excluding events with much energy lost by initial state radiation (ISR). The rejected background consists to a large degree of two photon events. It uses cuts on event multiplicity, on visible energy and longitudinal momentum balance. The cuts are documented in [2, 25–27].

So called good tracks and calorimeter clusters are identified by appropriate criteria [8]. Double counting of energy from charged tracks and calorimeter clusters is avoided by subtracting the estimated contribution of a charged track from the associated cluster energy.

The number of selected events for each energy point is given in Table 3.1.

3.5 Corrections to the data

The data are corrected further for the effects of limited detector acceptance and resolution, and residual ISR following [8]. All selected charged tracks, as well as the electromagnetic calorimeter clusters remaining after the correction for double counting of energy as described above, are used in the evaluation of the event shape moments. The values of the moments after the application of all selection cuts are said to be at the detector level.

As the QCD predictions are calculated for massless quarks we have to correct our data for the presence of events

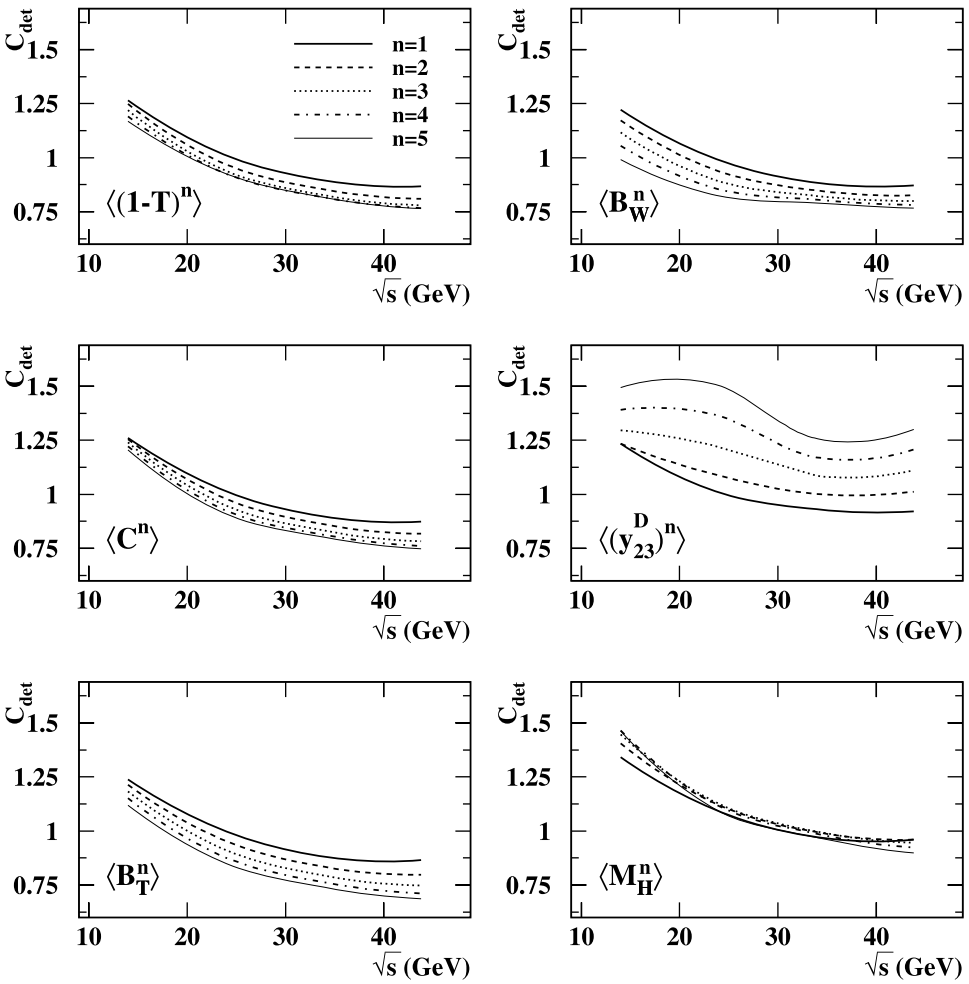

Fig. 3.1 Detector correction factors C_{det} as calculated using the PYTHIA MC model (see text for details). Line types correspond to moment order as shown in *top left* figure

originating from $b\bar{b}$ final states. Especially at low $\sqrt{s}$ the large mass of the b quarks and of the subsequently produced and decaying B hadrons will influence the values of the event shape variables. Therefore in the JADE analysis events from the process $e^+e^- \to b\bar{b}$ (approximately 1/11 of the hadronic events) are considered as background.

For the determination of the moments we calculate the sums $\sum_i y^n_{i,\mathrm{data}}$ (for moment order $n = 1, \ldots, 5$) where i counts all selected events. The expected contribution of $b\bar{b}$ background events $\sum_i y^n_{i,b\bar{b}}$, as estimated by PYTHIA, is subtracted from the observed sum $\sum_i y^n_{i,\mathrm{data}}$. By a multiplicative correction we then account for the effects of detector imperfections and of residual ISR and two photon background.

Two sets of sums $\sum_i y^n_i$ are calculated from MC simulated signal events. At detector level, MC events are treated identically to the data. The hadron level set is computed using the true momenta of the stable particles in the event,[4] and uses only events where $\sqrt{s'}$, the c.m. energy of the event, reduced due to ISR, satisfies $\sqrt{s} - \sqrt{s'} < 0.15$ GeV. The ratio of the MC hadron level moment over the MC detector level moment is applied as a detector correction factor for the data; the corrected sums are normalized by the corrected total number of selected events N_{tot} yielding the final values of $\langle y^n \rangle$,

$$\langle y^n \rangle^{\mathrm{had}} = \frac{\langle y^n \rangle^{\mathrm{had,MC}}}{\langle y^n \rangle^{\mathrm{det,MC}}} \cdot \left(\sum_i y^n_{i,\mathrm{det}} - \sum_i y^n_{i,b\bar{b}} \right) \Big/ N_{\mathrm{tot}}. \quad (3.1)$$

The corrected total number of events is calculated from the number of selected events in the data in the same way as for the moments.

There is some disagreement between the detector corrections calculated using PYTHIA or HERWIG at low $\sqrt{s}$ while at larger $\sqrt{s}$ the correction factors agree well for most observables. The difference in detector corrections will be evaluated as an experimental systematic uncertainty, see Sect. 4. The detector correction factors $C_{\mathrm{det}} = \langle y^n \rangle^{\mathrm{had,MC}} / \langle y^n \rangle^{\mathrm{det,MC}}$ as determined using PYTHIA are shown in Fig. 3.1.

4 Systematic uncertainties

Several contributions to the experimental uncertainties are estimated by repeating the analysis with varied track or event selection cuts or varied procedures as in [8]. For each systematic variation the value of the event shape moment or of α_S is determined and then compared to the default value. The experimental systematic uncertainty quoted is the result of adding in quadrature all contributions. In the fits of the QCD predictions to the data two further systematic uncertainties are evaluated:

- Using HERWIG 6.2 and ARIADNE 4.11 instead of PYTHIA 6.158 we assess the uncertainties associated with the hadronisation correction (Sect. 5.2). The hadronisation systematic uncertainty is defined by the larger change in α_S resulting from these alternatives.
- By varying the renormalisation scale factor x_μ we assess the theoretical uncertainty associated with missing higher order terms in the theoretical prediction. The renormalisation scale factor x_μ is set to 2.0 and 0.5. The theoretical systematic uncertainty is defined by the larger deviation from the default value.

5 Results

5.1 Values of event shape moments

The first five moments of the six event shape variables after subtraction of $b\bar{b}$ background and correction for detector effects measured by JADE are listed in Tables 5.1 and 5.2 and shown in Figs. 5.1 and 5.2. Superimposed we show the moments predicted by the PYTHIA, HERWIG and ARIADNE MC models tuned by OPAL to LEP 1 data. The moments become smaller by approximately one order of magnitude with each increasing moment order; the higher moments are more strongly suppressed with centre-of-mass energy. Statistical and experimental systematic uncertainties strongly increase with moment order.

In order to make a clearer comparison between data and models the lower plots in Figs. 5.1 and 5.2 show the differences between data and each model divided by the combined statistical and experimental error for $\sqrt{s} = 14$ and 35 GeV. The three models are seen to describe the data fairly well; PYTHIA and ARIADNE are found to agree better with the data than HERWIG.

5.2 Determination of α_S

In order to measure the strong coupling α_S, we fit the QCD predictions to the corrected moment values $\langle y^n \rangle$, i.e. to the data shown in Tables 5.1 and 5.2. The theoretical predictions using the $\mathcal{O}(\alpha_S^2)$ calculation described in Sect. 2 provide values at the parton level. It is necessary to correct for hadronisation effects in order to compare the theory with the hadron level data. Therefore the moments are calculated at hadron and parton level using large samples of PYTHIA 6.158 events and, as a cross check, samples obtained by simulation with HERWIG 6.2 and ARIADNE 4.11. Parton level is the stage at the end of the parton shower in the simulation of an hadronic event. In order to correct for hadronisation the data points are then multiplied by the ratio $C^{\mathrm{had}} = \langle y^n \rangle^{\mathrm{part,MC}} / \langle y^n \rangle^{\mathrm{had,MC}}$ of the parton over hadron level moments; $\langle y^n \rangle^{\mathrm{part}} = C^{\mathrm{had}} \cdot \langle y^n \rangle^{\mathrm{had}}$.

[4] All charged and neutral particles with a lifetime larger than 3×10^{-10} s are considered stable.

Table 5.1 Moments of the $1-T$, C, B_{T}, B_{W}, y_{23}^{D} and M_{H} distributions measured by JADE at 14.0, 22.0 and 34.6 GeV. The first uncertainty is statistical, while the second is systematic

n	$\langle(1-T)^n\rangle$ at 14.0 GeV	$\langle(1-T)^n\rangle$ at 22.0 GeV	$\langle(1-T)^n\rangle$ at 34.6 GeV
1	$(1.405 \pm 0.022 \pm 0.050) \cdot 10^{-1}$	$(1.123 \pm 0.021 \pm 0.028) \cdot 10^{-1}$	$(8.99 \pm 0.07 \pm 0.13) \cdot 10^{-2}$
2	$(2.38 \pm 0.08 \pm 0.17) \cdot 10^{-2}$	$(1.700 \pm 0.068 \pm 0.086) \cdot 10^{-2}$	$(1.192 \pm 0.020 \pm 0.024) \cdot 10^{-2}$
3	$(4.68 \pm 0.28 \pm 0.54) \cdot 10^{-3}$	$(3.31 \pm 0.21 \pm 0.26) \cdot 10^{-3}$	$(2.151 \pm 0.057 \pm 0.052) \cdot 10^{-3}$
4	$(1.04 \pm 0.09 \pm 0.17) \cdot 10^{-3}$	$(7.79 \pm 0.69 \pm 0.84) \cdot 10^{-4}$	$(4.77 \pm 0.17 \pm 0.16) \cdot 10^{-4}$
5	$(2.55 \pm 0.33 \pm 0.56) \cdot 10^{-4}$	$(2.08 \pm 0.24 \pm 0.29) \cdot 10^{-4}$	$(1.202 \pm 0.056 \pm 0.061) \cdot 10^{-4}$
n	$\langle C^n\rangle$ at 14.0 GeV	$\langle C^n\rangle$ at 22.0 GeV	$\langle C^n\rangle$ at 34.6 GeV
1	$(5.22 \pm 0.05 \pm 0.13) \cdot 10^{-1}$	$(4.280 \pm 0.057 \pm 0.077) \cdot 10^{-1}$	$(3.512 \pm 0.020 \pm 0.043) \cdot 10^{-1}$
2	$(3.00 \pm 0.06 \pm 0.14) \cdot 10^{-1}$	$(2.152 \pm 0.056 \pm 0.075) \cdot 10^{-1}$	$(1.561 \pm 0.018 \pm 0.030) \cdot 10^{-1}$
3	$(1.85 \pm 0.06 \pm 0.13) \cdot 10^{-1}$	$(1.235 \pm 0.047 \pm 0.064) \cdot 10^{-1}$	$(8.31 \pm 0.14 \pm 0.19) \cdot 10^{-2}$
4	$(1.22 \pm 0.05 \pm 0.11) \cdot 10^{-1}$	$(7.86 \pm 0.39 \pm 0.54) \cdot 10^{-2}$	$(5.04 \pm 0.11 \pm 0.13) \cdot 10^{-2}$
5	$(8.39 \pm 0.45 \pm 0.96) \cdot 10^{-2}$	$(5.41 \pm 0.33 \pm 0.46) \cdot 10^{-2}$	$(3.335 \pm 0.088 \pm 0.099) \cdot 10^{-2}$
n	$\langle B_{\mathrm{T}}^n\rangle$ at 14.0 GeV	$\langle B_{\mathrm{T}}^n\rangle$ at 22.0 GeV	$\langle B_{\mathrm{T}}^n\rangle$ at 34.6 GeV
1	$(1.918 \pm 0.017 \pm 0.038) \cdot 10^{-1}$	$(1.627 \pm 0.018 \pm 0.021) \cdot 10^{-1}$	$(1.372 \pm 0.006 \pm 0.011) \cdot 10^{-1}$
2	$(3.94 \pm 0.07 \pm 0.16) \cdot 10^{-2}$	$(2.963 \pm 0.067 \pm 0.077) \cdot 10^{-2}$	$(2.202 \pm 0.021 \pm 0.033) \cdot 10^{-2}$
3	$(8.61 \pm 0.26 \pm 0.54) \cdot 10^{-3}$	$(6.01 \pm 0.21 \pm 0.24) \cdot 10^{-3}$	$(4.082 \pm 0.062 \pm 0.083) \cdot 10^{-3}$
4	$(1.99 \pm 0.09 \pm 0.17) \cdot 10^{-3}$	$(1.344 \pm 0.065 \pm 0.072) \cdot 10^{-3}$	$(8.56 \pm 0.18 \pm 0.22) \cdot 10^{-4}$
5	$(4.84 \pm 0.28 \pm 0.55) \cdot 10^{-4}$	$(3.26 \pm 0.20 \pm 0.22) \cdot 10^{-4}$	$(1.978 \pm 0.053 \pm 0.062) \cdot 10^{-4}$
n	$\langle B_{\mathrm{W}}^n\rangle$ at 14.0 GeV	$\langle B_{\mathrm{W}}^n\rangle$ at 22.0 GeV	$\langle B_{\mathrm{W}}^n\rangle$ at 34.6 GeV
1	$(1.166 \pm 0.011 \pm 0.019) \cdot 10^{-1}$	$(1.000 \pm 0.012 \pm 0.014) \cdot 10^{-1}$	$(8.720 \pm 0.047 \pm 0.087) \cdot 10^{-2}$
2	$(1.482 \pm 0.031 \pm 0.048) \cdot 10^{-2}$	$(1.151 \pm 0.030 \pm 0.033) \cdot 10^{-2}$	$(9.42 \pm 0.11 \pm 0.20) \cdot 10^{-3}$
3	$(2.045 \pm 0.070 \pm 0.098) \cdot 10^{-3}$	$(1.525 \pm 0.065 \pm 0.068) \cdot 10^{-3}$	$(1.238 \pm 0.023 \pm 0.042) \cdot 10^{-3}$
4	$(3.04 \pm 0.15 \pm 0.19) \cdot 10^{-4}$	$(2.30 \pm 0.14 \pm 0.15) \cdot 10^{-4}$	$(1.897 \pm 0.050 \pm 0.085) \cdot 10^{-4}$
5	$(4.81 \pm 0.33 \pm 0.38) \cdot 10^{-5}$	$(3.84 \pm 0.32 \pm 0.36) \cdot 10^{-5}$	$(3.25 \pm 0.11 \pm 0.18) \cdot 10^{-5}$
n	$\langle (y_{23}^{\mathrm{D}})^n\rangle$ at 14.0 GeV	$\langle (y_{23}^{\mathrm{D}})^n\rangle$ at 22.0 GeV	$\langle (y_{23}^{\mathrm{D}})^n\rangle$ at 34.6 GeV
1	$(3.54 \pm 0.12 \pm 0.19) \cdot 10^{-2}$	$(2.89 \pm 0.12 \pm 0.10) \cdot 10^{-2}$	$(2.408 \pm 0.042 \pm 0.041) \cdot 10^{-2}$
2	$(2.55 \pm 0.22 \pm 0.29) \cdot 10^{-3}$	$(2.55 \pm 0.23 \pm 0.18) \cdot 10^{-3}$	$(2.173 \pm 0.081 \pm 0.049) \cdot 10^{-3}$
3	$(3.01 \pm 0.48 \pm 0.48) \cdot 10^{-4}$	$(3.93 \pm 0.55 \pm 0.37) \cdot 10^{-4}$	$(3.35 \pm 0.19 \pm 0.13) \cdot 10^{-4}$
4	$(4.7 \pm 1.2 \pm 1.0) \cdot 10^{-5}$	$(7.6 \pm 1.4 \pm 0.8) \cdot 10^{-5}$	$(6.42 \pm 0.48 \pm 0.38) \cdot 10^{-5}$
5	$(8.8 \pm 3.0 \pm 2.5) \cdot 10^{-6}$	$(1.66 \pm 0.36 \pm 0.21) \cdot 10^{-5}$	$(1.38 \pm 0.13 \pm 0.11) \cdot 10^{-5}$
n	$\langle M_{\mathrm{H}}^n\rangle$ at 14.0 GeV	$\langle M_{\mathrm{H}}^n\rangle$ at 22.0 GeV	$\langle M_{\mathrm{H}}^n\rangle$ at 34.6 GeV
1	$(3.207 \pm 0.024 \pm 0.049) \cdot 10^{-1}$	$(2.832 \pm 0.026 \pm 0.036) \cdot 10^{-1}$	$(2.522 \pm 0.010 \pm 0.024) \cdot 10^{-1}$
2	$(1.074 \pm 0.017 \pm 0.033) \cdot 10^{-1}$	$(8.55 \pm 0.16 \pm 0.21) \cdot 10^{-2}$	$(6.979 \pm 0.057 \pm 0.095) \cdot 10^{-2}$
3	$(3.74 \pm 0.09 \pm 0.17) \cdot 10^{-2}$	$(2.74 \pm 0.08 \pm 0.10) \cdot 10^{-2}$	$(2.114 \pm 0.028 \pm 0.030) \cdot 10^{-2}$
4	$(1.348 \pm 0.048 \pm 0.085) \cdot 10^{-2}$	$(9.36 \pm 0.40 \pm 0.49) \cdot 10^{-3}$	$(6.98 \pm 0.13 \pm 0.10) \cdot 10^{-3}$
5	$(5.02 \pm 0.24 \pm 0.41) \cdot 10^{-3}$	$(3.38 \pm 0.20 \pm 0.23) \cdot 10^{-3}$	$(2.485 \pm 0.062 \pm 0.051) \cdot 10^{-3}$

The models use cuts on quantities like e.g. the invariant mass between partons in order to regulate divergencies in the predictions for the parton shower evolution. As a consequence in some events no parton shower is simulated and the original quark-antiquark pair enters the hadronisation stage of the model directly. This leads to a bias in the calculation of moments at the parton level, since $y = 0$ in this case for all observables considered here (y_{23}^{D} cannot be calculated in this case). In order to avoid this bias we exclude in the simulation at the parton level events without gluon radiation, as in [28]. After this exclusion, the $\sqrt{s}$ evolution of the moments follows the QCD prediction; the change of the pre-

Table 5.2 Moments of the $1-T$, C, B_{T}, B_{W}, y_{23}^{D} and M_{H} distributions measured by JADE at 35.0, 38.3 and 43.8 GeV. The first uncertainty is statistical, while the second is systematic

n	$\langle(1-T)^n\rangle$ at 35.0 GeV	$\langle(1-T)^n\rangle$ at 38.3 GeV	$\langle(1-T)^n\rangle$ at 43.8 GeV
1	$(9.22 \pm 0.07 \pm 0.18) \cdot 10^{-2}$	$(9.06 \pm 0.19 \pm 0.22) \cdot 10^{-2}$	$(8.07 \pm 0.12 \pm 0.10) \cdot 10^{-2}$
2	$(1.260 \pm 0.019 \pm 0.045) \cdot 10^{-2}$	$(1.266 \pm 0.056 \pm 0.061) \cdot 10^{-2}$	$(1.032 \pm 0.032 \pm 0.024) \cdot 10^{-2}$
3	$(2.34 \pm 0.06 \pm 0.11) \cdot 10^{-3}$	$(2.41 \pm 0.16 \pm 0.17) \cdot 10^{-3}$	$(1.867 \pm 0.093 \pm 0.069) \cdot 10^{-3}$
4	$(5.36 \pm 0.17 \pm 0.29) \cdot 10^{-4}$	$(5.56 \pm 0.50 \pm 0.53) \cdot 10^{-4}$	$(4.22 \pm 0.29 \pm 0.23) \cdot 10^{-4}$
5	$(1.394 \pm 0.058 \pm 0.084) \cdot 10^{-4}$	$(1.44 \pm 0.16 \pm 0.17) \cdot 10^{-4}$	$(1.099 \pm 0.098 \pm 0.084) \cdot 10^{-4}$
n	$\langle C^n\rangle$ at 35.0 GeV	$\langle C^n\rangle$ at 38.3 GeV	$\langle C^n\rangle$ at 43.8 GeV
1	$(3.582 \pm 0.019 \pm 0.057) \cdot 10^{-1}$	$(3.486 \pm 0.056 \pm 0.065) \cdot 10^{-1}$	$(3.178 \pm 0.034 \pm 0.032) \cdot 10^{-1}$
2	$(1.620 \pm 0.017 \pm 0.047) \cdot 10^{-1}$	$(1.587 \pm 0.048 \pm 0.052) \cdot 10^{-1}$	$(1.347 \pm 0.028 \pm 0.025) \cdot 10^{-1}$
3	$(8.76 \pm 0.13 \pm 0.34) \cdot 10^{-2}$	$(8.76 \pm 0.38 \pm 0.39) \cdot 10^{-2}$	$(7.05 \pm 0.22 \pm 0.18) \cdot 10^{-2}$
4	$(5.38 \pm 0.10 \pm 0.25) \cdot 10^{-2}$	$(5.49 \pm 0.30 \pm 0.30) \cdot 10^{-2}$	$(4.25 \pm 0.17 \pm 0.14) \cdot 10^{-2}$
5	$(3.60 \pm 0.08 \pm 0.19) \cdot 10^{-2}$	$(3.74 \pm 0.25 \pm 0.24) \cdot 10^{-2}$	$(2.81 \pm 0.14 \pm 0.11) \cdot 10^{-2}$
n	$\langle B_{\mathrm{T}}^n\rangle$ at 35.0 GeV	$\langle B_{\mathrm{T}}^n\rangle$ at 38.3 GeV	$\langle B_{\mathrm{T}}^n\rangle$ at 43.8 GeV
1	$(1.395 \pm 0.006 \pm 0.016) \cdot 10^{-1}$	$(1.364 \pm 0.018 \pm 0.019) \cdot 10^{-1}$	$(1.260 \pm 0.011 \pm 0.010) \cdot 10^{-1}$
2	$(2.277 \pm 0.020 \pm 0.054) \cdot 10^{-2}$	$(2.229 \pm 0.059 \pm 0.064) \cdot 10^{-2}$	$(1.920 \pm 0.035 \pm 0.031) \cdot 10^{-2}$
3	$(4.30 \pm 0.06 \pm 0.15) \cdot 10^{-3}$	$(4.27 \pm 0.17 \pm 0.18) \cdot 10^{-3}$	$(3.480 \pm 0.098 \pm 0.087) \cdot 10^{-3}$
4	$(9.20 \pm 0.17 \pm 0.42) \cdot 10^{-4}$	$(9.30 \pm 0.51 \pm 0.54) \cdot 10^{-4}$	$(7.26 \pm 0.28 \pm 0.26) \cdot 10^{-4}$
5	$(2.17 \pm 0.05 \pm 0.12) \cdot 10^{-4}$	$(2.23 \pm 0.15 \pm 0.16) \cdot 10^{-4}$	$(1.681 \pm 0.084 \pm 0.080) \cdot 10^{-4}$
n	$\langle B_{\mathrm{W}}^n\rangle$ at 35.0 GeV	$\langle B_{\mathrm{W}}^n\rangle$ at 38.3 GeV	$\langle B_{\mathrm{W}}^n\rangle$ at 43.8 GeV
1	$(8.90 \pm 0.04 \pm 0.13) \cdot 10^{-2}$	$(8.76 \pm 0.13 \pm 0.17) \cdot 10^{-2}$	$(8.185 \pm 0.082 \pm 0.097) \cdot 10^{-2}$
2	$(9.83 \pm 0.10 \pm 0.31) \cdot 10^{-3}$	$(9.72 \pm 0.29 \pm 0.40) \cdot 10^{-3}$	$(8.73 \pm 0.19 \pm 0.22) \cdot 10^{-3}$
3	$(1.323 \pm 0.022 \pm 0.061) \cdot 10^{-3}$	$(1.319 \pm 0.062 \pm 0.087) \cdot 10^{-3}$	$(1.171 \pm 0.040 \pm 0.046) \cdot 10^{-3}$
4	$(2.08 \pm 0.05 \pm 0.12) \cdot 10^{-4}$	$(2.07 \pm 0.13 \pm 0.20) \cdot 10^{-4}$	$(1.859 \pm 0.089 \pm 0.100) \cdot 10^{-4}$
5	$(3.65 \pm 0.11 \pm 0.24) \cdot 10^{-5}$	$(3.60 \pm 0.30 \pm 0.50) \cdot 10^{-5}$	$(3.31 \pm 0.21 \pm 0.23) \cdot 10^{-5}$
n	$\langle (y_{23}^{\mathrm{D}})^n\rangle$ at 35.0 GeV	$\langle (y_{23}^{\mathrm{D}})^n\rangle$ at 38.3 GeV	$\langle (y_{23}^{\mathrm{D}})^n\rangle$ at 43.8 GeV
1	$(2.551 \pm 0.040 \pm 0.058) \cdot 10^{-2}$	$(2.66 \pm 0.12 \pm 0.16) \cdot 10^{-2}$	$(2.269 \pm 0.071 \pm 0.068) \cdot 10^{-2}$
2	$(2.395 \pm 0.080 \pm 0.071) \cdot 10^{-3}$	$(2.62 \pm 0.23 \pm 0.28) \cdot 10^{-3}$	$(2.10 \pm 0.14 \pm 0.11) \cdot 10^{-3}$
3	$(3.77 \pm 0.19 \pm 0.23) \cdot 10^{-4}$	$(4.04 \pm 0.52 \pm 0.61) \cdot 10^{-4}$	$(3.24 \pm 0.32 \pm 0.28) \cdot 10^{-4}$
4	$(7.31 \pm 0.48 \pm 0.71) \cdot 10^{-5}$	$(7.5 \pm 1.3 \pm 1.6) \cdot 10^{-5}$	$(6.19 \pm 0.82 \pm 0.77) \cdot 10^{-5}$
5	$(1.58 \pm 0.13 \pm 0.20) \cdot 10^{-5}$	$(1.52 \pm 0.34 \pm 0.44) \cdot 10^{-5}$	$(1.33 \pm 0.22 \pm 0.20) \cdot 10^{-5}$
n	$\langle M_{\mathrm{H}}^n\rangle$ at 35.0 GeV	$\langle M_{\mathrm{H}}^n\rangle$ at 38.3 GeV	$\langle M_{\mathrm{H}}^n\rangle$ at 43.8 GeV
1	$(2.555 \pm 0.009 \pm 0.018) \cdot 10^{-1}$	$(2.509 \pm 0.027 \pm 0.018) \cdot 10^{-1}$	$(2.371 \pm 0.017 \pm 0.026) \cdot 10^{-1}$
2	$(7.174 \pm 0.052 \pm 0.081) \cdot 10^{-2}$	$(7.00 \pm 0.15 \pm 0.11) \cdot 10^{-2}$	$(6.316 \pm 0.097 \pm 0.098) \cdot 10^{-2}$
3	$(2.209 \pm 0.026 \pm 0.035) \cdot 10^{-2}$	$(2.154 \pm 0.074 \pm 0.064) \cdot 10^{-2}$	$(1.884 \pm 0.047 \pm 0.034) \cdot 10^{-2}$
4	$(7.42 \pm 0.12 \pm 0.17) \cdot 10^{-3}$	$(7.22 \pm 0.35 \pm 0.39) \cdot 10^{-3}$	$(6.24 \pm 0.22 \pm 0.14) \cdot 10^{-3}$
5	$(2.694 \pm 0.060 \pm 0.091) \cdot 10^{-3}$	$(2.61 \pm 0.16 \pm 0.22) \cdot 10^{-3}$	$(2.26 \pm 0.11 \pm 0.07) \cdot 10^{-3}$

diction is comparable in size with the differences between employed MC generators. At the hadron and detector level all events are used.

The hadronisation correction factors C^{had} as obtained from PYTHIA 6.158 are shown in Fig. 5.3. We find that the hadronisation correction factors can be as large as two at low $\sqrt{s}$. For larger $\sqrt{s}$ the hadronisation corrections decrease as expected.

The models PYTHIA 6.158, HERWIG 6.2 and ARIADNE 4.11 do not agree well for moments based on B_{W}, y_{23}^{D} and M_{H} at low $\sqrt{s}$. The differences between the models are studied as a systematic uncertainty in the fits.

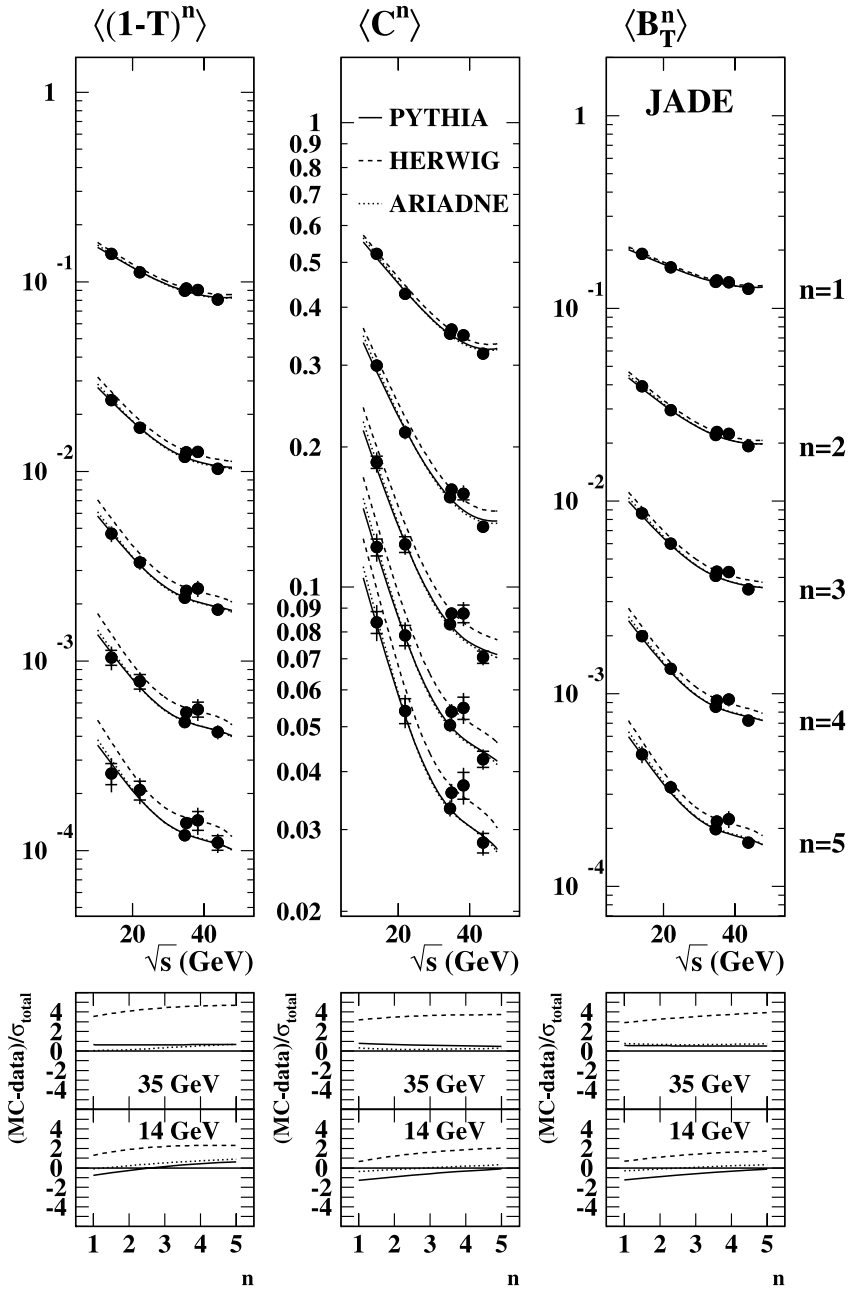

Fig. 5.1 First five moments of $1-T$, C and B_{T} at hadron level compared with predictions based on PYTHIA 6.158, HERWIG 6.2 and ARIADNE 4.11 MC events. The inner error bars—where visible—show the statistical errors, the outer bars show the total errors. Where no error bar is visible, the total error is smaller than the point size. The lower panels show the differences between data and MC at $\sqrt{s} = 14$ and 35 GeV, divided by the total error

A χ^2 value for each moment $\langle y^n \rangle$ is calculated using the formula

$$\chi^2 = \sum_i (\langle y^n \rangle_i^{\mathrm{part}} - \langle y^n \rangle_i^{\mathrm{part,theo}})^2 / \sigma_i^2, \tag{5.1}$$

where i counts the energy points, σ_i denotes the statistical errors and $\langle y^n \rangle^{\mathrm{part,theo}}$ is taken from (2.2).

The χ^2 value is minimized with respect to $\alpha_{\mathrm{S}}(M_{Z^0})$ for each moment n separately. The statistical uncertainty is found by varying the minimum value χ^2_{min} to $\chi^2_{\mathrm{min}} + 1$. The evolution of α_{S} from M_{Z^0} to c.m. energy $(\sqrt{s})_i$ is implemented in the fit in two-loop precision [29]. The renormalisation scale factor x_μ, as discussed in Sect. 2, is set to 1.

5.3 Fits of JADE data

Data and NLO prediction are compared, and this is repeated for every systematic variation. The results are shown in Fig. 5.4 and listed in Table 5.3. Figure 5.4 also contains the combination of the fit results discussed below. The values of χ^2/d.o.f. are in the order of 1–10, the fitted predictions—including the energy evolution of α_{S}—are consistent with

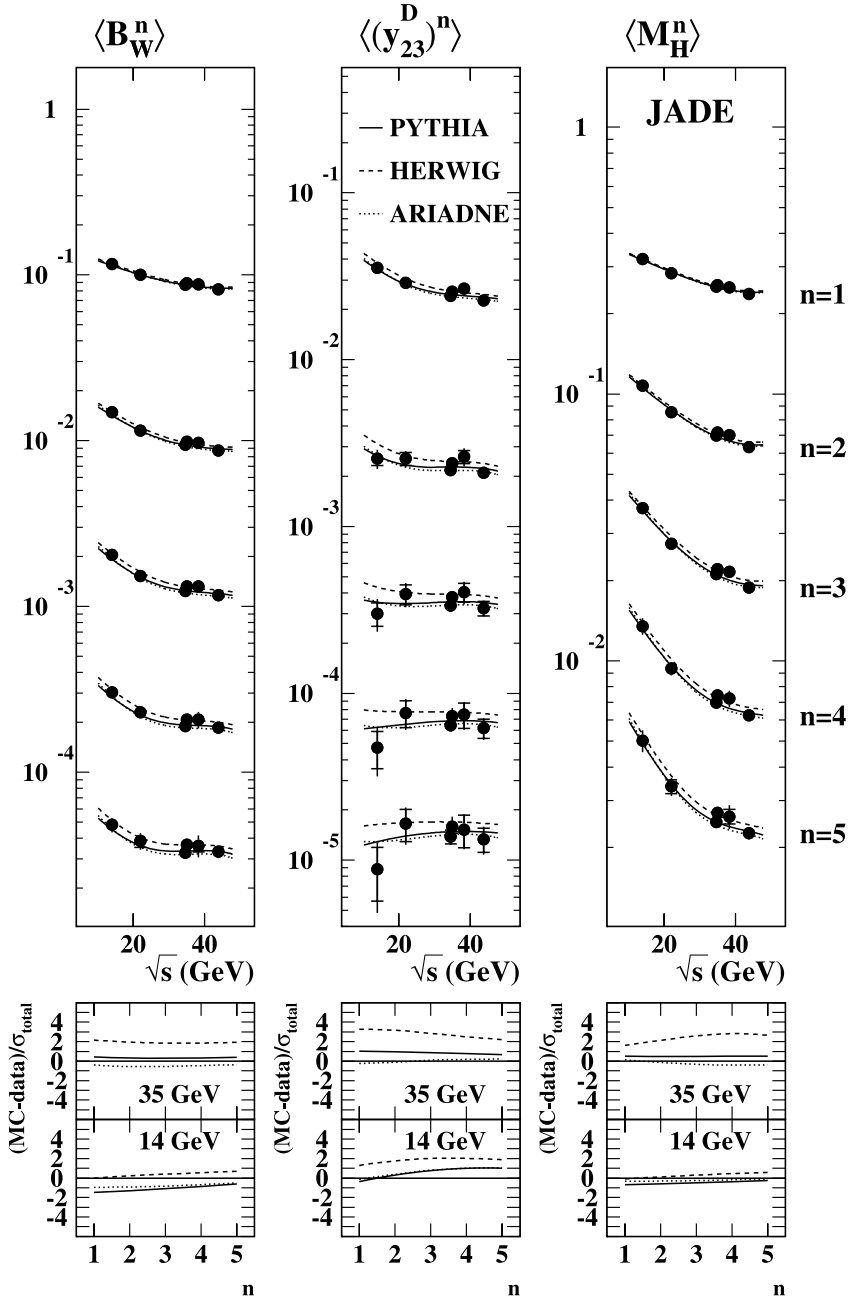

Fig. 5.2 First five moments of B_{W}, y_{23}^{D} and M_{H} at hadron level compared with predictions based on PYTHIA 6.158, HERWIG 6.2 and ARIADNE 4.11 MC events. The inner error bars—where visible—show the statistical errors, the outer bars show the total errors. Where no error bar is visible, the total error is smaller than the point size. The lower panels show the differences between data and MC at $\sqrt{s} = 14$ and 35 GeV, divided by the total error

the data. The fit to $\langle M_{\mathrm{H}}^1 \rangle$ does not converge and therefore no result is shown.[5]

The fitted values of $\alpha_{\mathrm{S}}(M_{\mathrm{Z}^0})$ increase steeply with the order n of the moment used, for $\langle (1-T)^n \rangle$, $\langle C^n \rangle$ and $\langle B_{\mathrm{T}}^n \rangle$. This effect is less pronounced and systematic for $\langle B_{\mathrm{W}}^n \rangle$, $\langle (y_{23}^{\mathrm{D}})^n \rangle$ and $\langle M_{\mathrm{H}}^n \rangle$. In Fig. 5.8 we show the ratio $K = \mathcal{B}_n/\mathcal{A}_n$ of NLO and LO coefficients for the six observables used in our fits to investigate the origin of this behaviour. Steeply increasing values of $\alpha_{\mathrm{S}}(M_{\mathrm{Z}^0})$ with moment order n for $\langle (1-T)^n \rangle$, $\langle C^n \rangle$ and $\langle B_{\mathrm{T}}^n \rangle$ and increasing values of K with n are clearly correlated. There is also a correlation with the rather large scale uncertainties in the respective fits. The other observables $\langle B_{\mathrm{W}}^n \rangle$, $\langle (y_{23}^{\mathrm{D}})^n \rangle$ and $\langle M_{\mathrm{H}}^n \rangle$ have more stable results for $\alpha_{\mathrm{S}}(M_{\mathrm{Z}^0})$ and correspondingly fairly constant values of K. The reason that the fit of $\langle M_{\mathrm{H}}^1 \rangle$ does not converge is the large and negative value of K.

[5]Equation (2.2) precludes a real solution $\bar{\alpha}_{\mathrm{S}}$, if $\mathcal{B}_n - 2\mathcal{A}_n < -\mathcal{A}_n^2/4\langle y^n \rangle$. For $\langle M_{\mathrm{H}}^1 \rangle$ this relation is fulfilled in the whole energy range 14–207 GeV, see Tables 5.1 and 5.2 and [7]. The NLO coefficient is negative in the case of $\langle B_{\mathrm{W}}^1 \rangle$, too. This observable gives the maximum value of $\chi^2/\mathrm{d.o.f.} = 98.5/5$, further problems in the determination of α_{S} using $\langle B_{\mathrm{W}}^1 \rangle$ show up in Sect. 5.4.

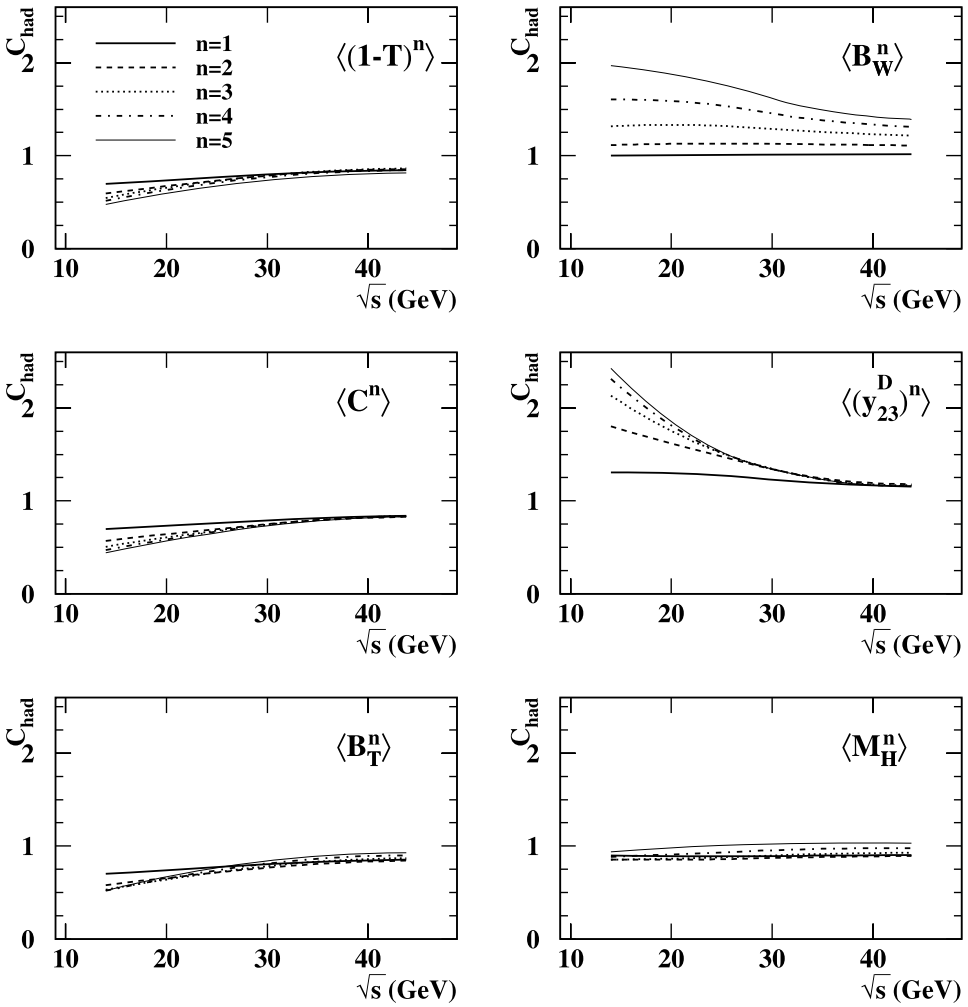

Fig. 5.3 Hadronisation correction factors C^{had} as calculated using the MC model PYTHIA 6.158 (see text for details). Line types correspond to moment order as shown in *top left* figure

5.4 Combined fits of JADE and OPAL data

For the most significant results we supplement the JADE data with the analogous OPAL data [7], covering the energy range of 91 to 209 GeV.

The JADE and OPAL detectors are very similar, both in construction and in the values of many detector parameters. The combined use of the JADE and OPAL data can therefore be expected to lead to consistent measurements, with small systematic differences. Our analysis procedure is therefore constructed to be similar to the one used in the OPAL analysis [7], in particular in the estimate of the systematic errors.

The central values and statistical errors of the combined fits are found employing the χ^2 calculation (5.1) as above.[6] However, the systematic uncertainties in this case cannot be found by simple repetitions of the fits, as the JADE and OPAL systematic variations are not identical.

[6]For this reason systematic differences between the two experiments contribute to the sometimes high χ^2 values; in Figs. 5.5 and 5.6 the experimental uncertainties are indicated separately.

The systematic uncertainties are correlated between different energy points, and including general correlations, the χ^2 calculation shown in (5.1) has to be generalised to [30]

$$\chi^2 = \sum_{i,j} (\langle y^n \rangle_i^{\mathrm{part}} - \langle y^n \rangle_i^{\mathrm{part,theo}}) \times V_{ij}^{-1} \cdot (\langle y^n \rangle_j^{\mathrm{part}} - \langle y^n \rangle_j^{\mathrm{part,theo}}), \tag{5.2}$$

where the V_{ij} are the covariances of the n-th moment at the energy points i and j. They have the form $V_{ij} = S_{ij} + E_{ij}$, with statistical covariances S_{ij} and experimental systematic covariances E_{ij}. The matrix S_{ij} is diagonal, $S_{ii} = \sigma^2_{\mathrm{stat.},i}$, as data of different energy points are independent. The experimental systematic covariances E_{ij} are only partly known:

– The diagonal entries are given by

$$E_{ii} = \sigma^2_{\mathrm{exp.},i},$$

denoting by $\sigma_{\mathrm{exp.},i}$ the experimental uncertainty at energy point i.

Table 5.3 Measurements of $\alpha_S(M_{Z^0})$ from event shape moments over the full analysed range of PETRA c.m. energies, 14–44 GeV. The hadronisation uncertainty is taken to be the larger of the deviations observed using HERWIG and ARIADNE

	$\langle(1-T)^1\rangle$	$\langle C^1\rangle$	$\langle B_T^1\rangle$	$\langle B_W^1\rangle$	$\langle(y_{23}^D)^1\rangle$	
$\alpha_S(M_{Z^0})$	0.1276	0.1241	0.1157	0.1308	0.1346	
Statistical error	0.0004	0.0003	0.0002	0.0004	0.0009	
Experimental syst.	0.0013	0.0010	0.0006	0.0014	0.0016	
HERWIG hadr. corr.	−0.0017	−0.0017	−0.0003	−0.0007	+0.0011	
ARIADNE hadr. corr.	+0.0002	+0.0000	+0.0009	−0.0042	−0.0051	
Hadronisation error	0.0017	0.0017	0.0009	0.0042	0.0051	
x_μ variation:						
$x_\mu = 2.0$	+0.0084	+0.0076	+0.0055	+0.0097	+0.0079	
$x_\mu = 0.5$	−0.0068	−0.0061	−0.0043	−0.0005	−0.0059	
χ^2/d.o.f.	14.9/5	16.7/5	48.8/5	98.8/5	40.0/5	
	$\langle(1-T)^2\rangle$	$\langle C^2\rangle$	$\langle B_T^2\rangle$	$\langle B_W^2\rangle$	$\langle(y_{23}^D)^2\rangle$	$\langle M_H^2\rangle$
$\alpha_S(M_{Z^0})$	0.1447	0.1417	0.1333	0.1327	0.1369	0.1294
Statistical error	0.0008	0.0005	0.0004	0.0006	0.0019	0.0004
Experimental syst.	0.0019	0.0017	0.0011	0.0021	0.0016	0.0011
HERWIG hadr. corr.	+0.0009	−0.0001	+0.0006	−0.0006	+0.0026	+0.0051
ARIADNE hadr. corr.	+0.0009	+0.0007	+0.0011	−0.0048	−0.0043	−0.0024
Hadronisation error	0.0009	0.0007	0.0011	0.0048	0.0043	0.0051
x_μ variation:						
$x_\mu = 2.0$	+0.0141	+0.0134	+0.0125	+0.0074	+0.0088	+0.0062
$x_\mu = 0.5$	−0.0113	−0.0109	−0.0103	−0.0055	−0.0067	−0.0043
χ^2/d.o.f.	13.5/5	16.3/5	33.7/5	64.7/5	13.7/5	92.7/5
	$\langle(1-T)^3\rangle$	$\langle C^3\rangle$	$\langle B_T^3\rangle$	$\langle B_W^3\rangle$	$\langle(y_{23}^D)^3\rangle$	$\langle M_H^3\rangle$
$\alpha_S(M_{Z^0})$	0.1514	0.1497	0.1434	0.1376	0.1352	0.1364
Statistical error	0.0013	0.0007	0.0007	0.0011	0.0030	0.0007
Experimental syst.	0.0022	0.0021	0.0014	0.0032	0.0027	0.0012
HERWIG hadr. corr.	+0.0033	+0.0016	+0.0018	−0.0006	+0.0033	+0.0069
ARIADNE hadr. corr.	+0.0016	+0.0015	+0.0012	−0.0059	−0.0039	−0.0030
Hadronisation error	0.0033	0.0016	0.0018	0.0059	0.0039	0.0069
x_μ variation:						
$x_\mu = 2.0$	+0.0166	+0.0164	+0.0162	+0.0084	+0.0084	+0.0087
$x_\mu = 0.5$	−0.0132	−0.0131	−0.0130	−0.0063	−0.0064	−0.0067
χ^2/d.o.f.	12.1/5	16.5/5	23.8/5	43.8/5	6.0/5	66.9/5
	$\langle(1-T)^4\rangle$	$\langle C^4\rangle$	$\langle B_T^4\rangle$	$\langle B_W^4\rangle$	$\langle(y_{23}^D)^4\rangle$	$\langle M_H^4\rangle$
$\alpha_S(M_{Z^0})$	0.1553	0.1546	0.1489	0.1392	0.1333	0.1399
Statistical error	0.0018	0.0009	0.0010	0.0019	0.0045	0.0010
Experimental syst.	0.0024	0.0024	0.0017	0.0042	0.0045	0.0013
HERWIG hadr. corr.	+0.0051	+0.0031	+0.0030	−0.0009	+0.0034	+0.0083
ARIADNE hadr. corr.	+0.0022	+0.0022	+0.0013	−0.0068	−0.0039	−0.0036
Hadronisation error	0.0051	0.0031	0.0030	0.0068	0.0039	0.0083
x_μ variation:						
$x_\mu = 2.0$	+0.0183	+0.0187	+0.0083	+0.0079	+0.0094	
$x_\mu = 0.5$	−0.0145	−0.0146	−0.0148	−0.0060	−0.0060	−0.0073
χ^2/d.o.f.	10.9/5	17.3/5	17.3/5	24.4/5	3.2/5	47.0/5

Table 5.3 (*Continued*)

	$\langle(1-T)^5\rangle$	$\langle C^5\rangle$	$\langle B_T^5\rangle$	$\langle B_W^5\rangle$	$\langle(y_{23}^D)^5\rangle$	$\langle M_H^5\rangle$
$\alpha_S(M_{Z^0})$	0.1580	0.1586	0.1525	0.1397	0.1314	0.1411
Statistical error	0.0027	0.0011	0.0015	0.0035	0.0070	0.0013
Experimental syst.	0.0029	0.0025	0.0020	0.0052	0.0061	0.0017
HERWIG hadr. corr.	+0.0066	+0.0044	+0.0040	−0.0013	+0.0031	+0.0094
ARIADNE hadr. corr.	+0.0027	+0.0029	+0.0012	−0.0077	−0.0043	−0.0040
Hadronisation error	0.0066	0.0044	0.0040	0.0077	0.0043	0.0094
x_μ variation:						
$x_\mu = 2.0$	+0.0198	+0.0204	+0.0206	+0.0078	+0.0075	+0.0096
$x_\mu = 0.5$	−0.0155	−0.0159	−0.0161	−0.0055	−0.0057	−0.0073
χ^2/d.o.f.	9.6/5	18.4/5	11.9/5	10.5/5	17.3/5	32.4/5

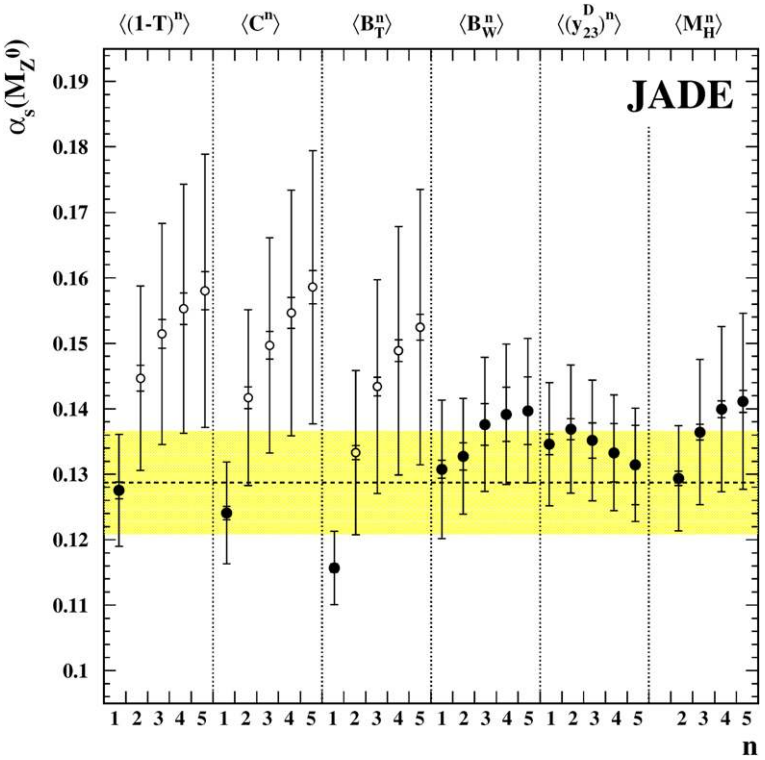

Fig. 5.4 Measurements of $\alpha_S(M_{Z^0})$ using fits to moments of six event shape variables at PETRA energies. The inner error bars—where visible—show the statistical errors, the outer bars show the total errors. The *dotted line* indicates the weighted average described in Sect. 5.5, the *shaded band* shows its error. Only the measurements indicated by *solid symbols* are used for this purpose

- The non diagonal entries can only follow from plausible assumptions. We employ the *minimum overlap assumption*[7]

$$E_{ij} = \mathrm{Min}\{\sigma^2_{\mathrm{exp.},i}, \sigma^2_{\mathrm{exp.},j}\}. \tag{5.3}$$

The total errors are found by fits employing the χ^2 calculation (5.2). We use the relative experimental uncertainties to determine the experimental uncertainties of the central values from the fits without correlations.

Figures 5.5 and 5.6 show the comparison of data points and predictions for the moments of the C-parameter and the wide jet broadening B_W. The predictions for $\langle C^n\rangle$ are seen to be in good agreement with the data and significantly confirm the QCD prediction of the energy dependence of $\alpha_S(\sqrt{s})$, also known as asymptotic freedom. The prediction slightly overshoots the higher moments of $1-T$, C and B_T at 14 GeV, and undershoots the moments of B_W, M_H, and sometimes y_{23}^D. At low $\sqrt{s}$ the NLO predictions of the B_W, y_{23}^D and M_H distributions are (unphysically) negative in a large range of the two jet region [15]. Therefore the NLO

[7]Fitting the low energy JADE points (14, 22 GeV) this assumption results [31] in a more accurate and more conservative error estimation than the *full overlap assumption* $E_{ij} = \mathrm{Max}\{\sigma^2_{\mathrm{exp.},i}, \sigma^2_{\mathrm{exp.},j}\}$ employed in [3].

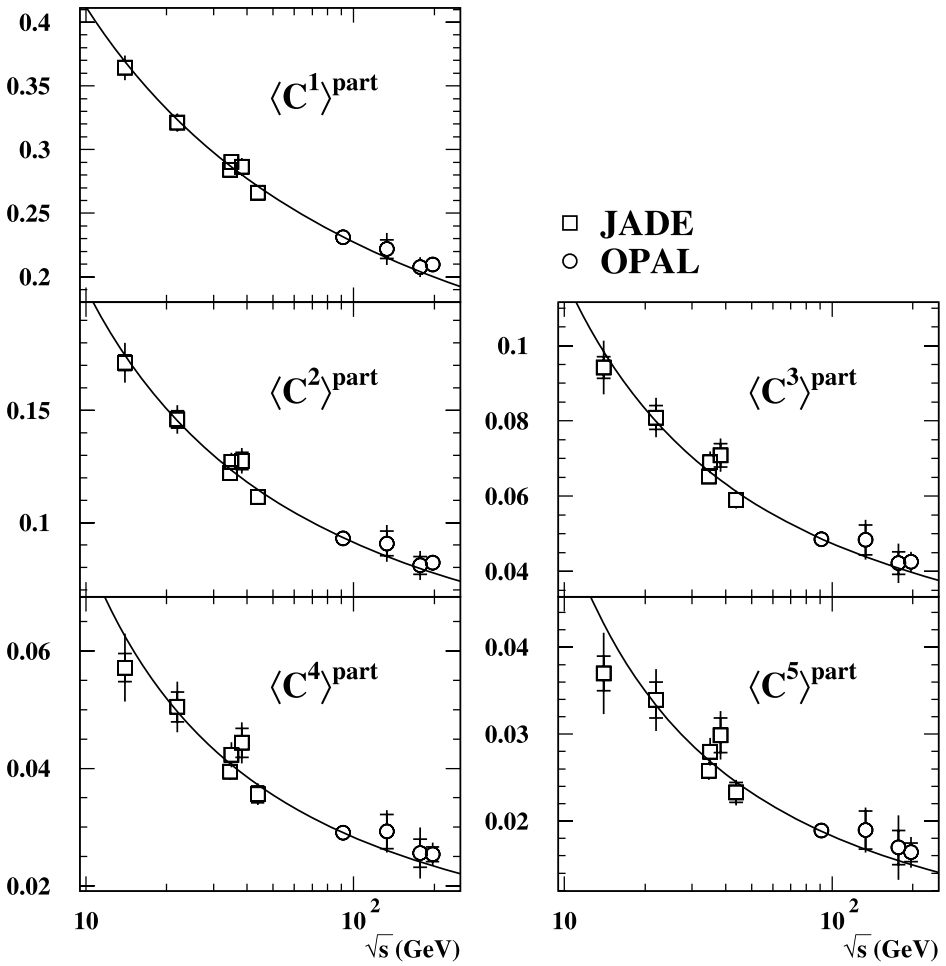

Fig. 5.5 Fits of the NLO predictions to JADE and OPAL measurements of moments of C at parton level. The *solid lines* show the $\sqrt{s}$ evolution of the NLO prediction based on the fitted value of $\alpha_S(M_{Z^0})$. The inner error bars—where visible—show the statistical errors used in the fit, the outer bars show the total errors. Where no error bar is visible, the total error is smaller than the point size

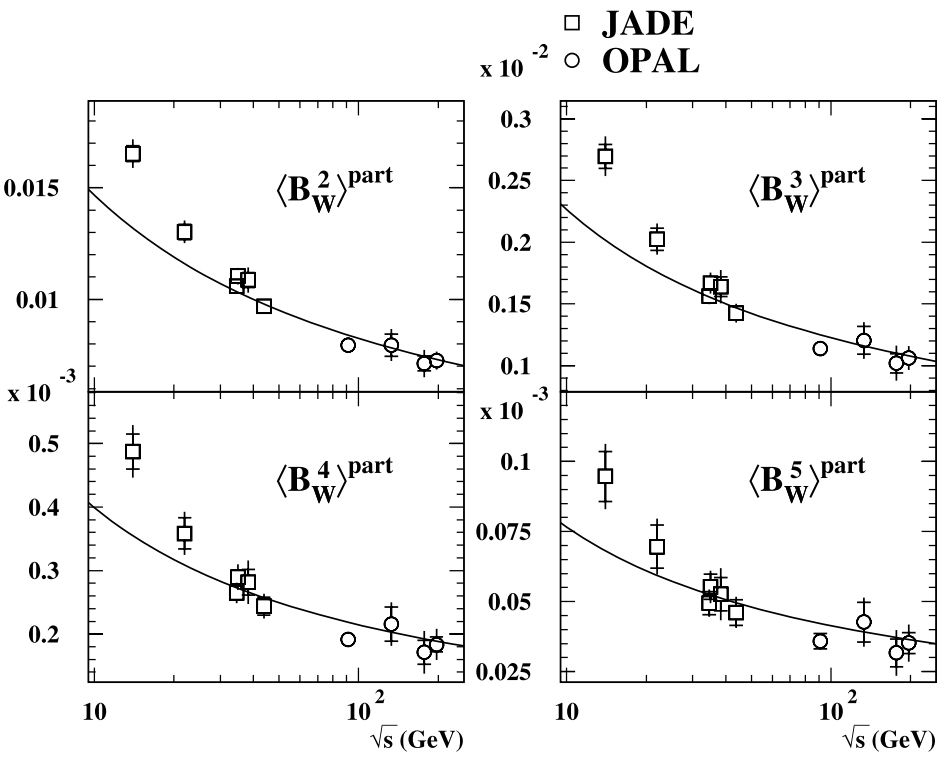

Fig. 5.6 Fits of the NLO predictions to JADE and OPAL measurements of moments of B_W at parton level. The *solid lines* show the $\sqrt{s}$ evolution of the NLO prediction based on the fitted value of $\alpha_S(M_{Z^0})$. The inner error bars—where visible—show the statistical errors used in the fit, the outer bars show the total errors. Where no error bar is visible, the total error is smaller than the point size. Problems of the NLO prediction at low $\sqrt{s}$ are discussed in the text

Table 5.4 Measurements of $\alpha_S(M_{Z^0})$ from event shape moments over the full analysed range of PETRA c.m. energies, 14–44 GeV, and the full range of LEP c.m. energies, 91–209 GeV. The hadronisation uncertainty is taken to be the larger of the deviations observed using HERWIG and ARIADNE. The experimental systematic errors is estimated by the minimum overlap assumption

	$\langle(1-T)^1\rangle$	$\langle C^1\rangle$	$\langle B_T^1\rangle$		$\langle(y_{23}^D)^1\rangle$	
$\alpha_S(M_{Z^0})$	0.1271	0.1242	0.1165		0.1259	
Statistical error	0.0002	0.0002	0.0001		0.0005	
Experimental syst.	0.0008	0.0006	0.0005		0.0016	
HERWIG hadr. corr.	−0.0017	−0.0020	−0.0014		+0.0006	
ARIADNE hadr. corr.	+0.0023	+0.0021	+0.0019		−0.0013	
Hadronisation error	0.0023	0.0021	0.0019		0.0013	
x_μ variation:						
$x_\mu = 2.0$	+0.0078	+0.0071	+0.0053		+0.0060	
$x_\mu = 0.5$	−0.0063	−0.0057	−0.0041		−0.0045	
χ^2/d.o.f.	31.2/9	36.1/9	114/9		173/9	
	$\langle(1-T)^2\rangle$	$\langle C^2\rangle$	$\langle B_T^2\rangle$	$\langle B_W^2\rangle$	$\langle(y_{23}^D)^2\rangle$	$\langle M_H^2\rangle$
$\alpha_S(M_{Z^0})$	0.1437	0.1414	0.1338	0.1271	0.1279	0.1253
Statistical error	0.0005	0.0003	0.0003	0.0004	0.0012	0.0003
Experimental syst.	0.0013	0.0011	0.0008	0.0013	0.0022	0.0009
HERWIG hadr. corr.	+0.0007	−0.0002	−0.0002	−0.0009	+0.0018	+0.0034
ARIADNE hadr. corr.	+0.0026	+0.0026	+0.0019	−0.0021	−0.0009	+0.0003
Hadronisation error	0.0026	0.0026	0.0019	0.0021	0.0018	0.0034
x_μ variation:						
$x_\mu = 2.0$	+0.0131	+0.0126	+0.0122	+0.0061	+0.0066	+0.0052
$x_\mu = 0.5$	−0.0107	−0.0103	−0.0100	−0.0045	−0.0051	−0.0036
χ^2/d.o.f.	22.3/9	24.7/9	47.0/9	230/9	46.4/9	247/9
	$\langle(1-T)^3\rangle$	$\langle C^3\rangle$	$\langle B_T^3\rangle$	$\langle B_W^3\rangle$	$\langle(y_{23}^D)^3\rangle$	$\langle M_H^3\rangle$
$\alpha_S(M_{Z^0})$	0.1509	0.1495	0.1436	0.1317	0.1282	0.1307
Statistical error	0.0010	0.0005	0.0005	0.0009	0.0021	0.0004
Experimental syst.	0.0016	0.0014	0.0011	0.0020	0.0025	0.0012
HERWIG hadr. corr.	+0.0026	+0.0011	+0.0011	−0.0008	+0.0022	+0.0047
ARIADNE hadr. corr.	+0.0027	+0.0031	+0.0018	−0.0034	−0.0012	−0.0002
Hadronisation error	0.0027	0.0031	0.0018	0.0034	0.0022	0.0047
x_μ variation:						
$x_\mu = 2.0$	+0.0158	+0.0154	+0.0159	+0.0069	+0.0067	+0.0071
$x_\mu = 0.5$	−0.0127	−0.0125	−0.0128	−0.0052	−0.0051	−0.0055
χ^2/d.o.f.	15.9/9	22.0/9	28.8/9	117/9	16.0/9	194/9
	$\langle(1-T)^4\rangle$	$\langle C^4\rangle$	$\langle B_T^4\rangle$	$\langle B_W^4\rangle$	$\langle(y_{23}^D)^4\rangle$	$\langle M_H^4\rangle$
$\alpha_S(M_{Z^0})$	0.1555	0.1551	0.1490	0.1340	0.1284	0.1329
Statistical error	0.0015	0.0006	0.0009	0.0017	0.0036	0.0007
Experimental syst.	0.0020	0.0016	0.0014	0.0029	0.0040	0.0015
HERWIG hadr. corr.	+0.0043	+0.0022	+0.0023	−0.0009	+0.0024	+0.0056
ARIADNE hadr. corr.	+0.0030	+0.0037	+0.0016	−0.0046	−0.0019	−0.0008
Hadronisation error	0.0043	0.0037	0.0023	0.0046	0.0024	0.0056
x_μ variation:						
$x_\mu = 2.0$	+0.0179	+0.0177	+0.0185	+0.0070	+0.0067	+0.0076
$x_\mu = 0.5$	−0.0142	−0.0141	−0.0146	−0.0051	−0.0051	−0.0058
χ^2/d.o.f.	13.0/9	21.7/9	20.3/9	50.2/9	6.6/9	139/9

Table 5.4 (*Continued*)

	$\langle(1-T)^5\rangle$	$\langle C^5\rangle$	$\langle B_T^5\rangle$	$\langle B_W^5\rangle$	$\langle(y_{23}^D)^5\rangle$	$\langle M_H^5\rangle$
$\alpha_S(M_{Z^0})$	0.1588	0.1598	0.1528	0.1349	0.1277	0.1336
Statistical error	0.0024	0.0007	0.0014	0.0032	0.0058	0.0010
Experimental syst.	0.0029	0.0016	0.0019	0.0044	0.0065	0.0021
HERWIG hadr. corr.	+0.0059	+0.0031	+0.0034	−0.0012	+0.0024	+0.0062
ARIADNE hadr. corr.	+0.0032	+0.0042	+0.0014	−0.0056	−0.0025	−0.0013
Hadronisation error	0.0059	0.0042	0.0034	0.0056	0.0025	0.0062
x_μ variation:						
$x_\mu = 2.0$	+0.0197	+0.0198	+0.0206	+0.0067	+0.0065	+0.0076
$x_\mu = 0.5$	−0.0155	−0.0156	−0.0160	−0.0046	−0.0049	−0.0058
χ^2/d.o.f.	11.6/9	23.6/9	13.9/9	19.0/9	3.1/9	93.3/9

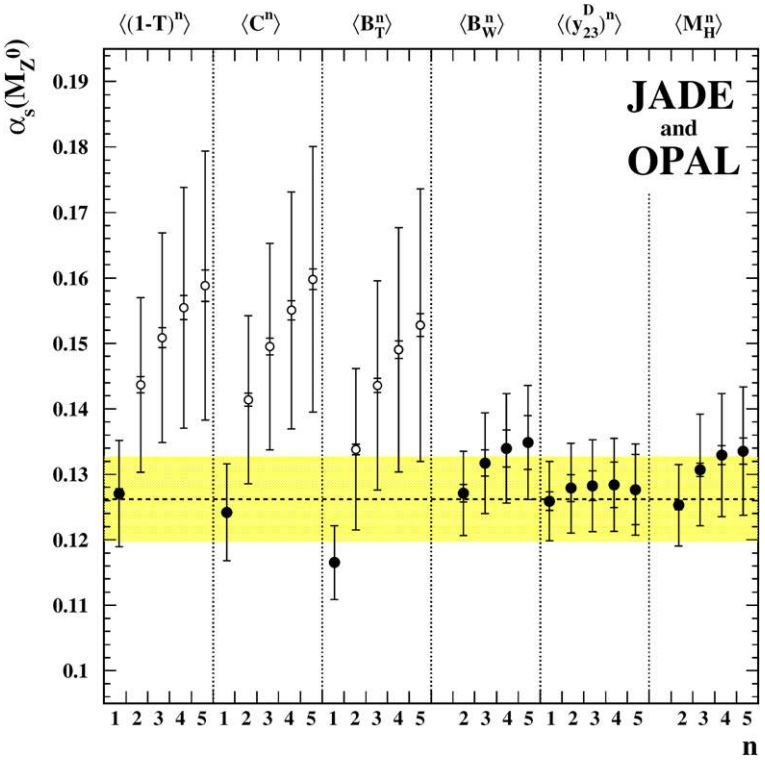

Fig. 5.7 Measurements of $\alpha_S(M_{Z^0})$ using fits to moments of six event shape variables at PETRA and LEP energies. The inner error bars—where visible—show the statistical errors, the outer bars show the total errors. The experimental systematic uncertainties are estimated by the minimum overlap assumption. The *dotted line* indicates the weighted average described in the text, the *shaded band* shows its error. Only the measurements indicated by *solid symbols* are used for this purpose

prediction for the moments is likely to be incomplete and too low to provide a satisfactory description of the data at low c.m. energies. In the case of $\langle B_W^1\rangle$ the α_S^2 coefficient is even negative, and we do not show or use this fit. The results are listed in Table 5.4 and shown in Fig. 5.7.

5.5 Combination of α_S determinations

To make full use of the data, we combine the measurements of $\alpha_S(M_{Z^0})$ from the various moments and event shapes and determine a single value. An extensive study was done by the LEP QCD working group on this problem [6, 7, 32–34], and their procedure is adopted here.

A weighted mean of the $\alpha_S(M_{Z^0})$ measurements is calculated which minimizes the χ^2 formed from the measurements and the combined value. This mean value, $\alpha_S(M_{Z^0})$, is given by

$$\alpha_S(M_{Z^0}) = \sum w_i \alpha_{S,i} \quad \text{with } w_i = \frac{\sum_j (V'^{-1})_{ij}}{\sum_{jk} (V'^{-1})_{jk}}, \qquad (5.4)$$

where the measured values of $\alpha_S(M_{Z^0})$ are denoted $\alpha_{S,i}$, their covariance matrix V', and the individual results are counted by i, j and k. The presence of highly correlated and dominant systematic errors makes a reliable estimate of V' difficult. Undesirable features (such as negative weights) can be caused by small uncertainties in the estimation of

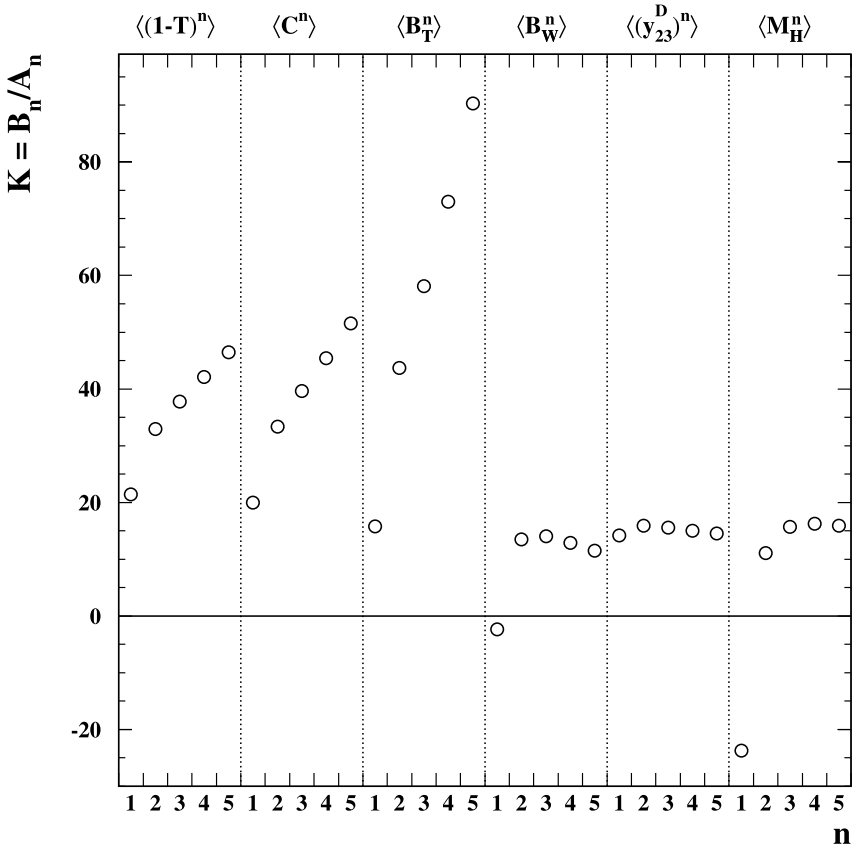

Fig. 5.8 The ratio $K = \mathcal{B}_n/\mathcal{A}_n$ of NLO and LO coefficients for the first five moments of the six event shape variables used in the determination of α_S, see also [7]

these correlations. Therefore only experimental systematic errors—assumed to be partially correlated by minimum overlap as $V'_{ij} = \min(\sigma^2_{\text{exp},i}, \sigma^2_{\text{exp},j})$—and statistical correlations are taken to contribute to the off-diagonal elements of the covariance matrix. The statistical correlations are determined using MC simulations at the parton level.[8] The diagonal elements are calculated from all error contributions—statistical, experimental, hadronisation and theory uncertainties. Using the weights derived from the covariance matrix V' the theory uncertainties are computed by analogously combining the $\alpha_S(M_{Z^0})$ values from setting $x_\mu = 2.0$ or $x_\mu = 0.5$, and the hadronisation uncertainties by combining the results obtained with the alternative hadronisation models.

To select observables with an apparently converging perturbative prediction, we consider [7] only those results for which the NLO term in (2.2) is less than half the corresponding LO term (i.e. $|K\alpha_S/2\pi| < 0.5$ or $|K| < 25$), namely $\langle 1-T\rangle$, $\langle C\rangle$, $\langle B_T\rangle$, $\langle B^n_W\rangle$ and $\langle (y^D_{23})^n\rangle$, $n = 1,\ldots,5$; and $\langle M^n_H\rangle$, $n = 2,\ldots,5$. These are results from 17 observables in total; or 16 observables from JADE and OPAL, excluding $\langle B^1_W\rangle$. The K values are shown in Fig. 5.8.

Using only JADE data, the result of the combination is

$$\alpha_S(M_{Z^0}) = 0.1287 \pm 0.0007(\text{stat.}) \pm 0.0011(\text{exp.}) \pm 0.0022(\text{had.}) \pm 0.0075(\text{theo.}),$$

and is shown in Fig. 5.4. Combining JADE and OPAL measurements, the result is

$$\alpha_S(M_{Z^0}) = 0.1262 \pm 0.0006(\text{stat.}) \pm 0.0010(\text{exp.}) \pm 0.0007(\text{had.}) \pm 0.0064(\text{theo.}),$$

and is shown in Fig. 5.7. Both values are above, but still consistent with the world average of $\alpha_S(M_{Z^0}) = 0.1189 \pm 0.0010$ [35]. It has been observed previously in comparisons of event shape distributions with NLO [36] or NNLO [37] QCD predictions with $x_\mu = 1$ that fitted values of $\alpha_S(M_{Z^0})$ tend to be large compared to the world average.

To enable comparison with earlier and more specific analyses [38] we combine the JADE fit results from only the first[9] moments $\langle 1-T\rangle$, $\langle C\rangle$, $\langle B_T\rangle$, $\langle B_W\rangle$, $\langle y^D_{23}\rangle$ and $\langle M^2_H\rangle$.

[8] The result is identical if the correlations are determined using PYTHIA, HERWIG or ARIADNE at 14.0…43.8 GeV, or determined at hadron level instead of parton level. The correlation values are cited in [31]; at 14 GeV and parton level they vary between 29% and 99% and are larger than 50% mostly.

[9] Because of the problems with the NLO description of $\langle M^1_H\rangle^{\text{part}}$, $\langle M^2_H\rangle$ is often regarded as the first moment of M_H.

This yields a value of

$$\alpha_S(M_{Z^0}) = 0.1243 \pm 0.0001(\text{stat.}) \pm 0.0009(\text{exp.}) \pm 0.0010(\text{had.}) \pm 0.0070(\text{theo.}).$$

The slightly smaller error in this determination of α_S reflects the fact that the lower order moments are less sensitive to the multijet region of the event shape distributions. This leads to a smaller statistical and theoretical uncertainty. In all three measurements the scale uncertainty is dominant.

6 Summary

In this paper we present measurements of moments of event shape distributions at centre-of-mass energies between 14 and 44 GeV using data of the JADE experiment. The predictions of the PYTHIA, HERWIG and ARIADNE MC models tuned by OPAL to LEP 1 data are found to be in reasonable agreement with the measured moments.

From fits of $\mathcal{O}(\alpha_S^2)$ predictions to selected event shape moments corrected for experimental and hadronisation effects we have determined the strong coupling to be $\alpha_S(M_{Z^0}) = 0.1287 \pm 0.0079$ (total error) using only JADE data, and $\alpha_S(M_{Z^0}) = 0.1262 \pm 0.0065$ (total error) using combined JADE and OPAL data. Fits to moments of M_H, B_W and y_{23}^D return large values of χ^2/d.o.f.; the higher moments, in particular of the $1-T$, C and B_T event shape variables, lead to systematically enlarged values of α_S. Results where α_S is steeply rising with moment order are strongly correlated with the relative size of the $\bar{\alpha}_S^2$ coefficient and thus are most likely affected by deficiencies of the NLO prediction.

The JADE experiment assesses an interesting energy range for the perturbative analysis since the energy evolution of the strong coupling is more pronounced at low energies.

Acknowledgements This research was supported by the DFG cluster of excellence 'Origin and Structure of the Universe'.

References

1. B. Naroska, Phys. Rep. **148**, 67 (1987)
2. JADE Coll., P.A. Movilla Fernández, O. Biebel, S. Bethke, S. Kluth, P. Pfeifenschneider et al., Eur. Phys. J. C **1**, 461 (1998)
3. JADE and OPAL Coll., P. Pfeifenschneider et al., Eur. Phys. J. C **17**, 19 (2000)
4. P. Movilla Fernández, in High Energy Physics ICHEP 2002, Proceedings of the 31st International Conference, ed. by S. Bentvelsen, P. de Jong, J. Koch, E. Laenen
5. O. Biebel, Phys. Rep. **340**, 165 (2001)
6. S. Kluth, Rep. Prog. Phys. **69**, 1771 (2006)
7. OPAL Coll., G. Abbiendi et al., Eur. Phys. J. C **40**, 287 (2005)
8. JADE Coll., J. Schieck, S. Bethke, O. Biebel, S. Kluth, P.A. Movilla Fernández, C. Pahl et al., Eur. Phys. J. C **48**, 3 (2006). Erratum-ibid.C50:769 (2007)
9. J. Schieck, in High Energy Physics ICHEP 2006, Proceedings of the 33rd International Conference, ed. by A. Sissakian, G. Kozlov, E. Kolganova
10. M. Dasgupta, G. Salam, J. Phys. G **30**, R143 (2004)
11. A. Gehrmann-De Ridder, T. Gehrmann, E.W.N. Glover, G. Heinrich, J. High Energy Phys. **12**, 094 (2007)
12. S. Weinzierl, Phys. Rev. Lett. **101**, 162001 (2008)
13. S. Catani, M. Seymour, Phys. Lett. B **378**, 287 (1996)
14. R. Ellis, D. Ross, A. Terrano, Nucl. Phys. B **178**, 421 (1981)
15. P. Movilla Fernández, Ph.D. thesis, RWTH Aachen (2003)
16. T. Sjöstrand, Comput. Phys. Commun. **82**, 74 (1994)
17. G. Marchesini et al., Comput. Phys. Commun. **67**, 465 (1992)
18. E. Elsen, JADE Computer Note, vol. 54, unpublished (1982)
19. E. Elsen, Ph.D. thesis, Universität Hamburg (1981)
20. C. Bowdery, J. Olsson, JADE Computer Note, vol. 73, unpublished (1984)
21. G. Corcella et al., J. High Energy Phys. **01**, 010 (2001)
22. L. Lönnblad, Comput. Phys. Commun. **71**, 15 (1992)
23. OPAL Coll., G. Alexander et al., Z. Phys. C **69**, 543 (1996)
24. OPAL Coll., G. Abbiendi et al., Eur. Phys. J. C **35**, 293 (2004)
25. JADE Coll., W. Bartel et al., Phys. Lett. B **88**, 171 (1979)
26. JADE Coll., W. Bartel et al., Phys. Lett. B **129**, 145 (1983)
27. JADE Coll., S. Bethke et al., Phys. Lett. B **213**, 235 (1988)
28. OPAL Coll., G. Abbiendi et al., Eur. Phys. J. C **53**, 21 (2008)
29. R. Ellis, W. Stirling, B. Webber, *Cambridge Monographs on Particle Physics, Nuclear Physics and Cosmology*, vol. 8 (Cambridge University Press, Cambridge, 1996)
30. Particle Data Group, W.-M. Yao et al., J. Phys. G **33**, 1 (2006)
31. C. Pahl, Ph.D. thesis. TU München (2007). http://nbn-resolving.de/urn:nbn:de:bvb:91-diss-20070906-627360-1-2
32. R.W.L. Jones, Nucl. Phys. Proc. Suppl. **133**, 13 (2004)
33. M. Ford, Ph.D. thesis, University of Cambridge (2004)
34. ALEPH Coll., A. Heister et al., Eur. Phys. J. C **35**, 457 (2004)
35. S. Bethke, Prog. Part. Nucl. Phys. **58**, 351 (2006)
36. OPAL Coll., P. Acton et al., Z. Phys. C **59**, 1 (1993)
37. G. Dissertori et al., J. High Energy Press **0802**, 040 (2008)
38. JADE Coll., P.A. Movilla Fernández, S. Bethke, O. Biebel, S. Kluth et al., Eur. Phys. J. C **22**, 1 (2001)